Van der Waals stacks of few-layer h-AlN with graphene: an ab initio study of structural, interaction and electronic properties

Renato B. dos Santos, F. de Brito Mota, R. Rivelino, Anelia Kakanakova-Gueorguie and Gueorgui Kustov Gueorguiev

Linköping University Post Print

Tweet

N.B.: When citing this work, cite the original article.

Van der Waals stacks of few-layer h-AlN with graphene: an *ab-initio* study of structural, interaction and electronic properties

Renato B. dos Santos[1,2], F. de Brito Mota[1], R. Rivelino[1], A. Kakanakova-Georgieva[2], and G. K. Gueorguiev[2]

[1]Instituto de Física, Universidade Federal da Bahia, 40210-340 Salvador, Bahia, Brazil

[2]Department of Physics, Chemistry and Biology (IFM), Linköping University,
581 83 Linköping, Sweden

Corresponding Author:
*E-mail: gekos@ifm.liu.se (G.K.G.)

Abstract

Graphite-like hexagonal AlN (h-AlN) multilayers have been experimentally manifested and theoretically modeled. The development of any functional electronics applications of h-AlN would most certainly require its integration with other layered materials, particularly graphene. Here, by employing vdW-corrected density functional theory calculations, we investigate structure, interaction energy, and electronic properties of van der Waals stacking sequences of few-layer h-AlN with graphene. We find that the presence of a substrate such as graphene induces enough interlayer charge separation in h-AlN, favoring a graphite-like stacking formation. We also find that the interface dipole, calculated per unit cell of the stacks, tends to increase with the number of stacked layers of h-AlN and graphene.

1. Introduction

Since the start of its intense research in the late 1980's [1], group III nitrides, including AlN, GaN, InN, and their alloys, has become one of the most extensively studied and most widely applied classes of semiconductor materials for the development of short wavelengths light emitting diodes (LEDs) and lasers (2014 Nobel Prize in Physics). Group III nitrides naturally crystalize in the wurtzite (wz) structure represented by two interpenetrating hexagonal sub-lattices of group III atoms and nitrogen atoms, respectively. Each group III atom forms four-fold coordination with nitrogen atoms and vice versa, adopting sp^3-hybridization of the bonds.

The wurtzite structure is referred to for bulk crystals of AlN and GaN grown for example by physical vapor transport (PVT) [2]; and thin films of group III nitrides grown for example by metal organic chemical vapor deposition (MOCVD) [3] and molecular beam epitaxy (MBE) on various substrates including sapphire, SiC, and Si as part of respective device heterostructures [4]. Group III nitrides naturally grow along the <0001> direction in the wurtzite structure. The wurtzite crystal structure of AlN (wz-AlN, respectively, wz-GaN and wz-InN) is commonly represented as stacking of bilayers along this direction. Each bilayer consists of two closely spaced hexagonal layers, one with Al (respectively, Ga or In) atoms and the other with N atoms [4].

For the first time experimental evidence for "graphite-like" hexagonal AlN (h-AlN) has been reported [5]. The ultrathin h-AlN (up to 12 layers in the stack) was prepared by MBE on substrates of single crystal Ag(111). Most recently, the initial formation of few-layer h-AlN on (111)Si surface by ammonia assisted MBE was investigated indicating transformation to the wz-AlN at a maximum thickness of 5-6 monolayers [6]. h-AlN refers to the prototype structure of h-BN [7], whereby each layer can be represented as a regular network of AlN hexagons. The alternating Al and N atoms in the AlN hexagons adopt three-fold coordination with sp^2-hybridization of the bonds. It has been demonstrated, by ab-initio density functional calculations, that the h-AlN structure can be preserved for up to about 24 layers; and that the relaxation to the wurtzite structure for larger number of layers is associated with a certain charge transfer [8]. Just recently, theoretical investigation of the number-of-layer-dependent structural, electronic and vibrational properties of h-AlN have been reported [9], whereby it has been predicted that an indirect-to-direct band gap transition occurs for stacks containing ten layers of h-AlN, which certainly has implications for any prospective device applications.

We have previously carried out modeling of a perfect single layer of h-AlN. Our theoretical study on the structural and electronic properties of single layers of h-AlN further involved the incorporation of selected point defects (e.g., vacancies, as well as substitutional atoms of silicon and carbon) providing the prospect for deliberate tailoring of its electronic properties [10]. Aspects of the structural and electronic properties of functionalized layers of h-AlN have also been calculated, indicating its potential for carbon dioxide capture and storage [11], and realization of "ferromagnetic order" towards application in room-temperature spintronics [12].

The development of any functional electronics applications of h-AlN would most certainly require its integration with other layered materials, particularly graphene. Most recently, the integration of group III nitrides with graphene involved the realization of van der Waals epitaxy of wz-GaN on epitaxial graphene, further MOCVD of InGaN/GaN heterostructures and demonstration of fully functional blue LEDs with application in flexible electronics by the release of the wz-GaN film and its transfer to a plastic tape [13]. The impact of graphene properties and the use of graphene as a potential template for the heteroepitaxy of wz-GaN and wz-AlN is further treated by other research groups [14].

In the present work, by employing vdW-corrected density functional theory (DFT) calculations, we investigate structure, interaction energy, and electronic properties of van der Waals stacking sequences of few-layer h-AlN with graphene; and find certain number-of-layer-dependent trends. We obtain the charge distribution at the h-AlN and graphene components of the stacks thus assessing the mechanisms responsible for their formation. By analyzing the interlayer energy interaction and difference in the electron-density charge for the corresponding stacks, we conclude the suitability of few-layer graphene as a substrate for few-layer h-AlN.

2. Methods and computational details

The relaxed structures and electronic properties of several stacks of few-layer h-AlN with graphene were calculated within the framework of density functional theory (DFT) including dispersion corrections, as implemented in the SIESTA package [15]. The exchange-correlation functional employed was based on the Perdew-Burke-Ernzerhof (PBE) approach [16]. The Kohn-Sham orbitals were expanded within double-ζ basis sets, including polarization functions, combined with the norm-conserving Troullier-Martins pseudopotentials [17] to treat the electron core interactions. The dispersion interactions, which play an important role in weakly interacting systems, such as the stacks considered in the present work, were included in our calculations by employing the DFT-D2 method as developed by Grimme [18]. For the global scaling factor (S_6) in the dispersion energy term, we have obtained the value of $S_6 = 1.0$. Employing this value in test calculations recurring to the well-studied h-BN as a reference system, we have reproduced the experimental values for the structural features, e.g., equilibrium inter-layer distance (d_0), and B-N bond length (L_{B-N}) for stacks of two layers of h-BN in AA' configuration [19].

The reciprocal space was sampled by a fine grid of 10x10x1 k-points [20] in the Brillouin zone of the unit cells. In order to ensure that the h-AlN components in all stacks of this work are dynamically stable, the phonon spectrum of single-layer h-AlN was obtained by making use of a fine grid of 45x45x1 k-points [15].

During the relaxation procedures of all stacks, a mesh cutoff energy of 500 Ry was applied to determine the self-consistent charge density, which provided a precision in the total energy of less than 0.4 meV per supercell. The stacks were considered optimized when the residual forces on the atoms decreased below the value of 0.02 eV/Å.

Stacking together few layers of h-AlN and graphene may lead to certain deviation of both h-AlN and graphene layers from their planarity. Such deviation from planarity is usually small (0.01 - 0.1 Å). It is perceived as a result of stress accommodation in the stacks due to the graphene and h-AlN lattice mismatch, and it is unrelated to the usual buckling parameter [21, 22] commonly defined for stacking sequences.

In all calculations, in order to avoid spurious interactions between the adjacent planes in different cells, we have considered a distance of 30 Å between such adjacent planes belonging to different cells.

3. Results and discussion

We have first performed reference calculations of the structural and electronic properties of single-layer h-AlN which involved obtaining the equilibrium structure (Fig. 1a), the respective in-plane lattice constant, bond length, cohesive energy, and band gap value. These characteristic parameters and values are listed in table 1 together with the respective values for a single-layer graphene. For the in-plane lattice constant of single-layer h-AlN we obtained the value of 3.17 Å, and an Al-N bond length of 1.83 Å. Any small discrepancies with our previously calculated values obtained at the PBE level of theory [10], are accounted for by the dispersion corrections implemented in the present calculations. The calculated value for the in-plane lattice constant of single-layer h-AlN agrees reasonably well with a recently reported calculated value of 3.13 Å [9]. The general trend is that the in-plane lattice constant of single-layer h-AlN is slightly larger than the in-plane lattice constant of 3.11 Å for wz-AlN [23]. Experimentally, the structural characterization of ultrathin h-AlN (12 single layers) yields an in-plane lattice

4

constant of 3.15 Å [5]. The following relationship between the lattice constant of the primitive cell of single-layer h-AlN ($a_{h\text{-}AlN}$ = 3.17 Å) and graphene (a_G = 2.49 Å) can be noticed: 4×$a_{h\text{-}AlN}$ ≈ 5×a_G. Such a simple integer-number ratio by permitting an easy construction of super-cell configurations for stacks of h-AlN with graphene greatly facilitates their theoretical modeling. The phonon spectrum of the single-layer h-AlN in the whole BZ, Fig.1 (b), does not exhibit any imaginary frequencies, and this result confirms its dynamical stability, in agreement with the analysis of the vibrational properties of single-layer h-AlN reported by Şahin et al. [22].

Table 1. Calculated lattice constant (a), Al-N bond length ($L_{Al\text{-}N}$), C-C bond length ($L_{C\text{-}C}$), cohesive energy per atom (E_{coh}/at), and energy band gap (E_g) for a single-layer h-AlN and graphene. The cohesive energy per atom $E_{coh/at}$ is defined as $E_{coh/at} = [E_{tot} − (n_N E_N + n_{Al} E_{Al})]/(n_N + n_{Al})$, where E_{tot} is the total energy of the model system, n_N and n_{Al} are the numbers of N and Al atoms per unit cell, and E_N and E_{Al} are the energies of the isolated N and Al species, respectively. Similarly, in the case of graphene, $E_{coh/at} = (E_{tot} − n_C E_C)/n_C$ where E_{tot} is the total energy of the model system, n_C is the number of C atoms per unit cell, and E_C is the energy of the isolated C atoms.

System	a (Å)	$L_{Al\text{-}N/C\text{-}C}$ (Å)	E_{coh}/at (eV)	E_g (eV)
h-AlN	3.17 3.13[a]	1.83 1.81[a]	5.05 5.36[a]	2.88 2.9[a]
Graphene	2.49 2.46	1.44 1.42[b]	7.92	0.00

[a] Ref. 10.

[b] Review of C-C bond lengths and cohesive energy values relevant to graphene obtained by calculations and experiments can be found in Ref. 24.

We provide the partial density of electronic states (PDOS), figure 1(c), as well as the band structure of a single-layer h-AlN, figure 1(d), for completeness of the reference calculations. The PDOS, calculated with spin polarization (figure 1(c)) indicate that there is no net magnetic

moment in the system, as expected for a single h-AlN layer. Furthermore, as inferred by analyzing the components of the calculated orbital projections, the top of valence band (TVB) is formed by $2p_z$-orbitals of the N atoms, and the bottom of conduction band (BCB) is formed by 2s-orbitals of the N atoms belonging to the h-AlN layer, which is similar, to some extent, to the charge density distribution of a single-layer h-BN [25]. It is worth mentioning that the characteristics of the valence band dispersion of a single-layer h-AlN (figure 1(c)) indicate its potential as a 2D material with an indirect band gap with states localized in N atoms. Contrastingly, in the case of graphene both TVB and BCB are formed by $2p_z$-orbitals of the C atoms, thus exhibiting totally delocalized states [26]. This electronic difference between single-layer h-AlN and graphene makes them electronically alternative single-layer building blocks for van der Waals stacks and corresponding devices.

We obtain that a single-layer h-AlN exhibits an indirect band gap of 2.88 eV (Fig. 1d). The good agreement of the properties of single-layer h-AlN obtained here with previous studies dedicated to this system [9, 10], emphasizes the appropriateness of the level of theory chosen in this work for modeling stacks of h-AlN with graphene.
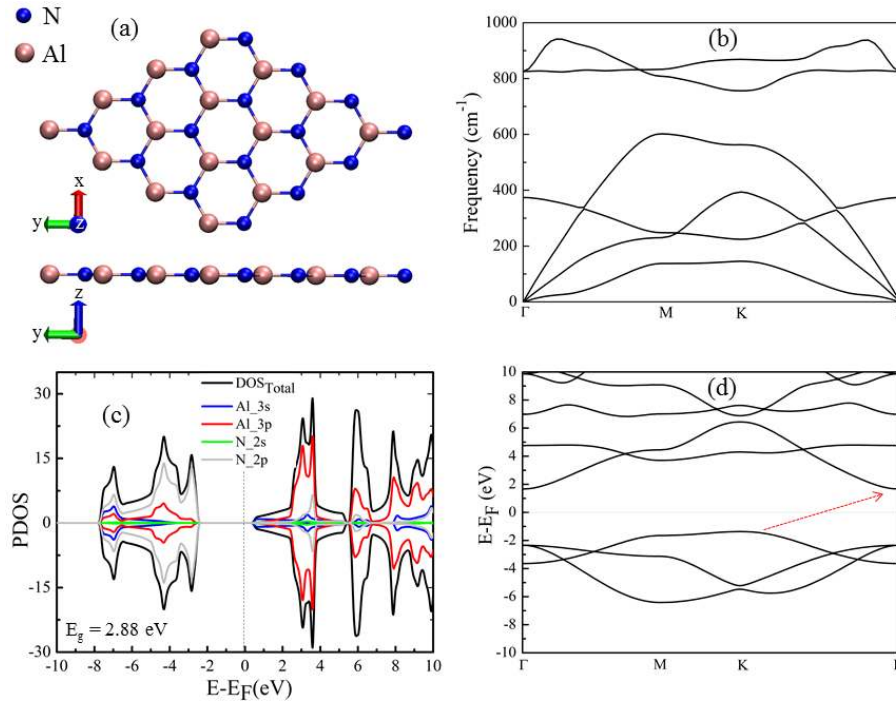

Figure 1. Single-layer h-AlN: (a) an optimized 3x3x1 atomic layer; (b) calculated phonon dispersion; (c) partial density of electronic states (PDOS) calculated with spin polarization; and (d) band structure (red arrow between TVB and BCB indicates the indirect band gap of single-layer h-AlN).

Two-layer h-AlN can adopt five different stacking configurations following commonly introduced stacking configurations and notations [9]: two stacking configurations result as the hexagons of one layer reside on the hexagons of the other layer, e.g., Al over Al and N over N (AA), and Al over N and N over Al (AA'); other three stacking configurations result as the hexagons of one layer are translated with respect to the hexagons of the other layer, e.g., AB, AB', and A'B, Fig. 2 (a). The AA' stacking configuration has been calculated to be the "ground-state stacking order" out of the five possible stacking configurations [9], and confirmed in our calculations. It can be judged by the largest value of the interlayer binding energy, $E_b = 292.03$ meV/at (table 2) defined as $E_b = |E_{bilayer} - 2E_{monolayer}|/M$, where M is the total number of atoms in the stack. As displayed in figure 2(b), the p_z-orbital of the N atoms from one of the h-AlN layers interacts with the p_z-orbital of the Al atoms from the other layer. This results in a charge localization between N and Al atoms belonging to different layers which leads to a strongly bound stack with interlayer distance $d_0 = 2.18$ Å, which is smaller compared to both bilayers of h-BN and graphene, respectively (table 2). The calculated electron density difference $\Delta\rho = \rho_{bilayer\ h-AlN} - (2\rho_{h-AlN})$ shown in figure 2(b) illustrates how the formation of the stack of two-layer h-AlN (in its most stable stacking configuration AA') perturbs the electronic structure of the single-layers h-AlN.

The AA' stacking configuration has been reported as the most energetically favorable for h-GaN [27] and h-BN [19] as well. However, while the AA' and AB configurations for two-layer h-BN are energetically close and they may coexist at experimental conditions [19], the AA' configuration for two-layer h-AlN is by far the most stable following the values of the interlayer binding energy reported in table 2.
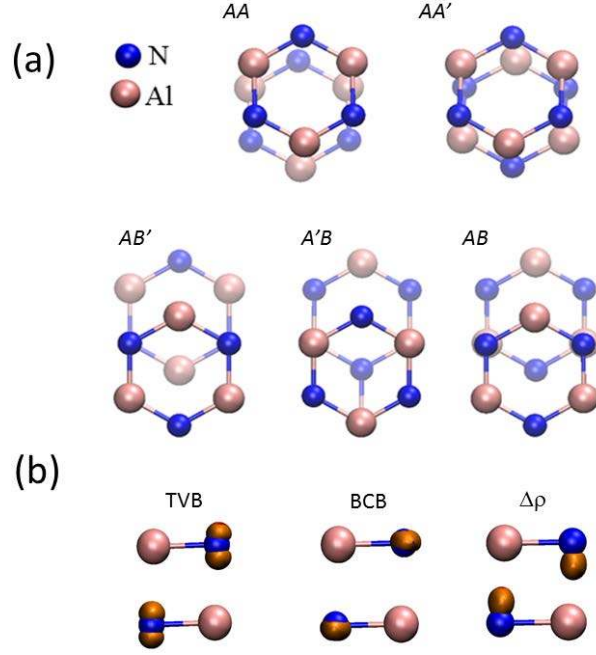
Figure 2. (a) Stacking configurations for two-layer h-AlN; (b) the Kohn-Sham charge densities at TVB and BCB and the corresponding electron density difference $\Delta\rho$ resulting from the stacking of two-layer h-AlN in the case of the most stable stacking configuration AA'.

Table 2. Calculated inter-layer distances (d_0) and corresponding binding energies (E_b) for two-layer h-AlN. The calculated values for two-layer h-BN and graphene in their most stable configurations *AA'* and *AB*, respectively, are included for comparative purposes.

Two-layer	stacking	d_0 (Å)	E_b (meV/at)
h-AlN	AA	3.76	32.14
	AA'	2.18	292.03
	AB	2.63	124.73
	A'B	3.43	47.75
	AB'	3.55	40.63
h-BN	AA'	3.25 3.25[a]	32.21
Graphene	AA	3.31	39.74
	AB	3.09 3.33[b]	50.63

(a) Ref. 19.

(b) Ref. 24.

We next explore the structural, interaction and electronic properties of several different stacking sequences of few-layer h-AlN with graphene. These are displayed in figure 3, whereby h-AlN and graphene assumes the energetically most favorable configuration AA', and AB, respectively. The various stacking configurations involve up to three-layer h-AlN, and up to three-layer graphene. Particularly, the number of graphene layers (one and up to three) can be well-controlled for epitaxial graphene which is formed by high-temperature sublimation process on the Si-face of SiC [28] and opens up an experimentally feasible approach for van der Waals epitaxy of h-AlN on graphene. Certain theoretical calculations model the effect of graphene on the structural and electronic properties of h-BN [29, 30], and in more general context the effect of substrate on the electronic properties of silicene [31]. Here, we contribute new knowledge considering for the first time the stacks of few-layer h-AlN with graphene, their configuration and their van der Waals type of interaction leading to perseverance of the electronic properties of h-AlN when part of such stacks.
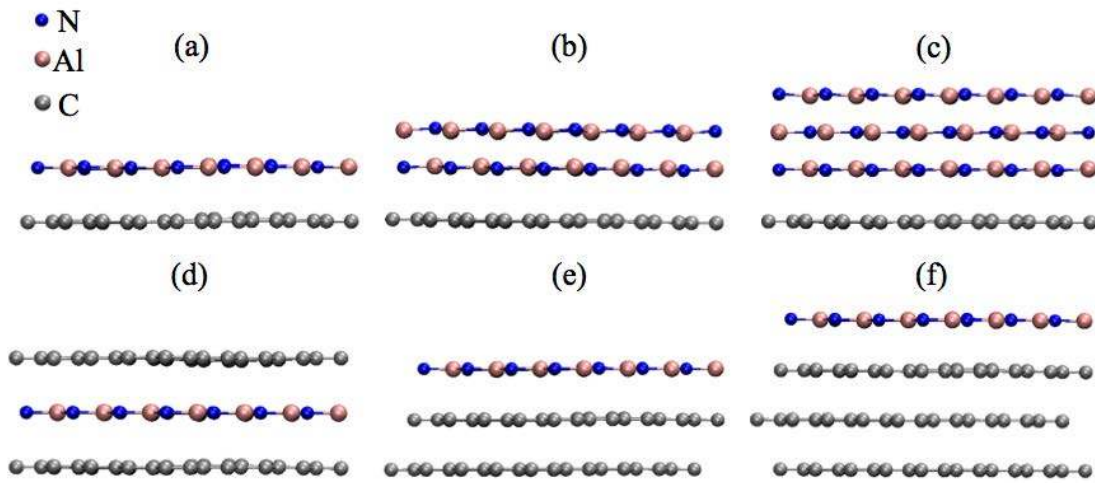

Figure 3. Different stacking configurations of few-layer h-AlN and graphene labeled here (and further in text) as stack I (a), stack II (b), stack III (c), stack IV (d), stack V (e), and stack VI (f). See main text for detailed description of these stacks.

The optimized stacking configuration of single-layer h-AlN on graphene is displayed in figure 4. The supercell corresponding to such van der Waals heterostructure exhibits a lattice parameter that corresponds to $4 \times a_{h\text{-}AlN} \approx 5 \times a_G$ and equals to 12.52 Å (reported also in table 3).

Consequently, in stack I, the lattice constant of the graphene layer undergoes a slight stretching of ca. 0.05 Å, while the lattice constant of the single-layer h-AlN contracts by ca. 0.15 Å. However, after full relaxation there is no obvious buckling either of the single-layer h-AlN or graphene layer. The calculated binding energy per atom of stack I is of 70 meV/at and the corresponding equilibrium interlayer distance is 3.13 Å. This binding energy is larger than the corresponding value for a two-layer graphene (E_b = 50.63 eV/at) in its most favorable *AB* configuration, albeit it is smaller than the binding energy per atom we calculated in the present work for two-layer h-AlN (E_b = 292.03 eV/at) in its most favorable *AA'* configuration (table 2).
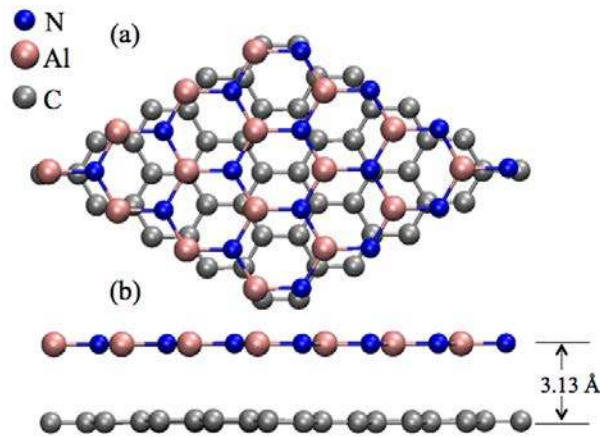

Figure 4. Optimized stacking configuration for stack I (single-layer h-AlN on a graphene layer): (a) top and (b) side view.

The structural, energetic, and dipolar properties of all vdW heterostructures (stacks I–VI) are summarized in table 3. Reviewing structural features such as supercell parameters and bond lengths for stacks I–III (table 3), suggests that the three-layer h-AlN preserves to a significant extent the structural properties of single-layer h-AlN. In general, those stacks comprising larger number of h-AlN layers than graphene layers, e.g., stack III, have lattice constant value of about $4 \times a_{h\text{-}AlN}$. Stacks comprising larger number of graphene layers, e.g., stacks V and VI, are found to have lattice constant of about $5 \times a_G$. Since the particular sandwich-like stacking sequence IV is, to a large extent, defined by the (external) graphene layers, it naturally exhibits structural parameters very similar to those of single-layer graphene. In general, stress/extension of the h-AlN layers resulting from their interplay with the graphene layers influences the supercell parameter a in the stacks. However, these variations are quite moderate (varying between 12.52 Å and 12.67 Å) reaching saturation (at a = 12.67 Å) for the case three h-AlN layers on a

graphene layer. Consequently, the structural variations between different stacks of few-layer h-AlN with graphene may be experimentally undetectable.

Table 3. Bond length (L), supercell lattice parameter (a), interlayer equilibrium distance (d_0), interaction energy (E_{int}^0 and E_{int}^*) and net electric dipole moment in the z-direction (μ) for all stacks I–VI (as displayed in figure 3).

stacks	Order	$L_{\text{Al-N}}$ (Å)	$L_{\text{C-C}}$ (Å)	a (Å)	d_0 (Å)	E_{int}^0 /E$^*_{int}$/(eV/layer)	μ (D)
I	h-AlN	1.81	—	12.52	3.13	–2.65 /-2.82/	3.60
	Graphene	—	1.45				
II	h-AlN (1)	1.83	—	12.66	2.20	–7.77 /-8.36/	3.69
	h-AlN (2)		—		3.09		
	graphene	—	1.46				
III	h-AlN (1)	1.83	—	12.67	2.21	–9.88 /-11.37/	4.07
	h-AlN (2)				2.20		
	h-AlN (3)				3.10		
	graphene	—	1.47				
IV	graphene	—	1.44	12.49	3.15	–3.74 /-5.08/	0.00
	h-AlN	1.80	—		3.15		
	graphene	—	1.44				
V	h-AlN	1.80	—	12.49	3.11	–3.59 /-3.71/	4.17
	graphene (1)	—	1.44		3.08		
	graphene (2)						
VI	h-AlN	1.80	—	12.48	3.11	–4.07 /-4.18/	4.38
	graphene (1)	—			3.07		
	graphene (2)	—	1.44		3.07		
	graphene (3)						

For all stacks (I–VI), the value of the h-AlN–graphene inter-layer distance varies in the relatively narrow range between 3.09–3.15 Å. The h-AlN layer is located closer (3.09–3.10 Å) to the graphene layer in the stack containing two-layer h-AlN (stack II) and three-layer h-AlN (stack III), while the corresponding equilibrium inter-layer distance is larger in stacks containing more graphene layers (stack VI), as well as in the sandwich-like stack IV. On the other hand, the value of the graphene–graphene inter-layer distance in the stacks containing more than one graphene layer (stacks V and VI) keeps fairly constant as of 3.07–3.08 Å; and the value of the h-AlN–h-AlN inter-layer distance in the stacks containing more than one h-AlN layer (stacks II and III) keeps fairly constant as of 2.20–2.21 Å. However, the h-AlN – h-

AlN distances are much smaller than h-AlN – graphene and graphene – graphene inter-layer distances, which is an expression of the different chemical nature of the h-AlN layers (in comparison to graphene) tolerating closely packed stacks.

While a single-layer h-AlN exhibits a vanishing electric dipole moment, when it forms a stack with a graphene layer (stack I), a resulting dipole moment of $\mu = 3.60$ D per unit cell is obtained. Stacking together an h-AlN and a graphene layer unbalances the electron density at the interface of the stack, thus leading to a charge separation and a resulting dipole moment. The prevailing component of the dipole moment appears pointing from the h-AlN layer to the graphene layer (z-direction). Comparing all stacks (I–VI), the electric dipole moment in the z-direction increases by 13% (from 3.60 D to 4.07 D), as the number of h-AlN layers on top of graphene increases (stacks I–III); and by 22% (from 3.60 D to 4.38 D), as the number of graphene layers increases (stacks I, V and VI). More graphene layers lead to stronger polarization of the h-AlN layer(s) and a larger value of the interface dipole. Naturally, in the specific case of the sandwiched stack IV, the dipole moment vanishes. In this stack the graphene layers isolate (i.e., shield) the single-layer h-AlN.

It has been previously found for stacks of h-BN with graphene that the intrinsic interfacial dipole in that stack may originate from the work function mismatch and Pauli exchange repulsion, which leads to interface charge rearrangement [29]. The same work also suggests that the stack-induced dipole asymmetry may be used to control the doping of the h-BN/graphene interface without resorting to any external field, but exploiting instead the properties intrinsic to such stacks. Additionally, similar phenomenon has been previously employed [32] to tune the band gap of tri-layer graphene. We emphasize that a similar behavior is also consistent for the stacks of few-layer h-AlN with graphene reported in the present study.

Table 3 lists the calculated stacks' interaction energies, and defined as (i) the energy difference between a stack and its constituent layers $E^0_{int} = (E_{stack} - nE_{h-AlN0} - mE_{G0})/(n + m)$, where n and m corresponds to the number of h-AlN and graphene layers in the stack, and (ii) the energy difference between a stack and its constituent layers (exhibiting the same geometry as in the stack) $E^*_{int} = (E_{stack} - nE^*_{h-AlN} - mE^*_G)/(n + m)$. Both quantities are complementary by accounting, or do not accounting, respectively, for the structural modification of the layers when assembled in the stacks. As seen in figure 5, both E^0_{int} and E^*_{int} exhibit a clear trend: when the number of graphene or h-AlN layers in the stack increases, the interaction energy turns more

negative, thus energetically favoring the stacking process. This favorable energetic trend indicates that graphene may be an appropriate substrate for growing few-layer h-AlN in a similar way as h-BN has been revealed as favorable substrate for growing silicene layers [31].
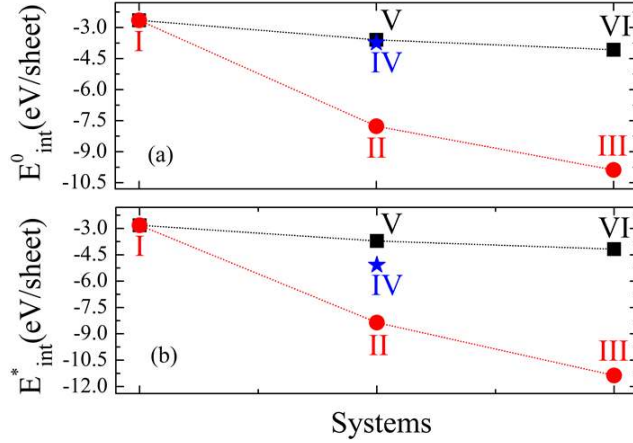

Figure 5. Interaction energies: (a) E^0_{int}, and (b) the E^*_{int} (see main text for definitions) for stacks I–IV (following their representation in figure 3). The roman numbers correspond to the stack's numbering in figure 3. Displayed in red are stacks I, II, and III, for which on a single-layer graphene, one to three h-AlN layers are stacked. Displayed in black are stacks V and VI, for which a single-layer h-AlN is stacked with graphene layers. Displayed in blue is the stack IV formed by single-layer h-AlN sandwiched between two graphene layers.

The projected density of states (PDOS) for all stacks I–VI is displayed in figure 6(a)–(f). The electronic states that most contribute to the TVB of the stacks are essentially provided by the p_z-orbitals of the N atoms of the h-AlN layers, whereas the electronic states that most contribute to the BCB are essentially given by the p_z-orbitals of the C atoms of graphene. Such electronic behavior is similar to the stacking of h-BN on graphene [30] even though the single-layer h-AlN and the single-layer h-BN differ significantly in such an important electronic property as the size of their band gaps. The h-AlN is a wide-band gap semiconductor with a calculated indirect band gap of 2.88 eV (table 1) while the h-BN is a typical insulator with a band gap of 4.59 eV [30].

To analyze the influence of the number of h-AlN and graphene layers on the charge distribution in the stacks I–VI, the electron density differences $\Delta\rho = \rho_{stack} - (\rho_{h\text{-}AlN} + \rho_G)$ is calculated and displayed below the PDOS graphs in figure 6 (a)–(f). The electron density is localized

predominantly between the layers of each stack, which illustrates the interaction mechanism keeping the stacks bound together. As indicated by the electron density differences, for two-layer h-AlN, the filled p_z-orbitals of the N atoms from one of the layers interact with the empty p_z-orbitals of the Al atoms from the other layer (see figure 2(b)). When a graphene layer is stacked with single-layer h-AlN (stack I), the filled p_z-orbitals of the N atoms in the h-AlN repel the semi-occupied p_z-orbitals of the graphene layer, while the empty p_z-orbitals of the Al atoms become available to interact with unpaired electrons from graphene (figure 6 (a)). A similar charge transfer mechanism is observed for all stacks I-VI, which is related to the formation of interface dipoles, which contributes to keeping the layers together in the stack.
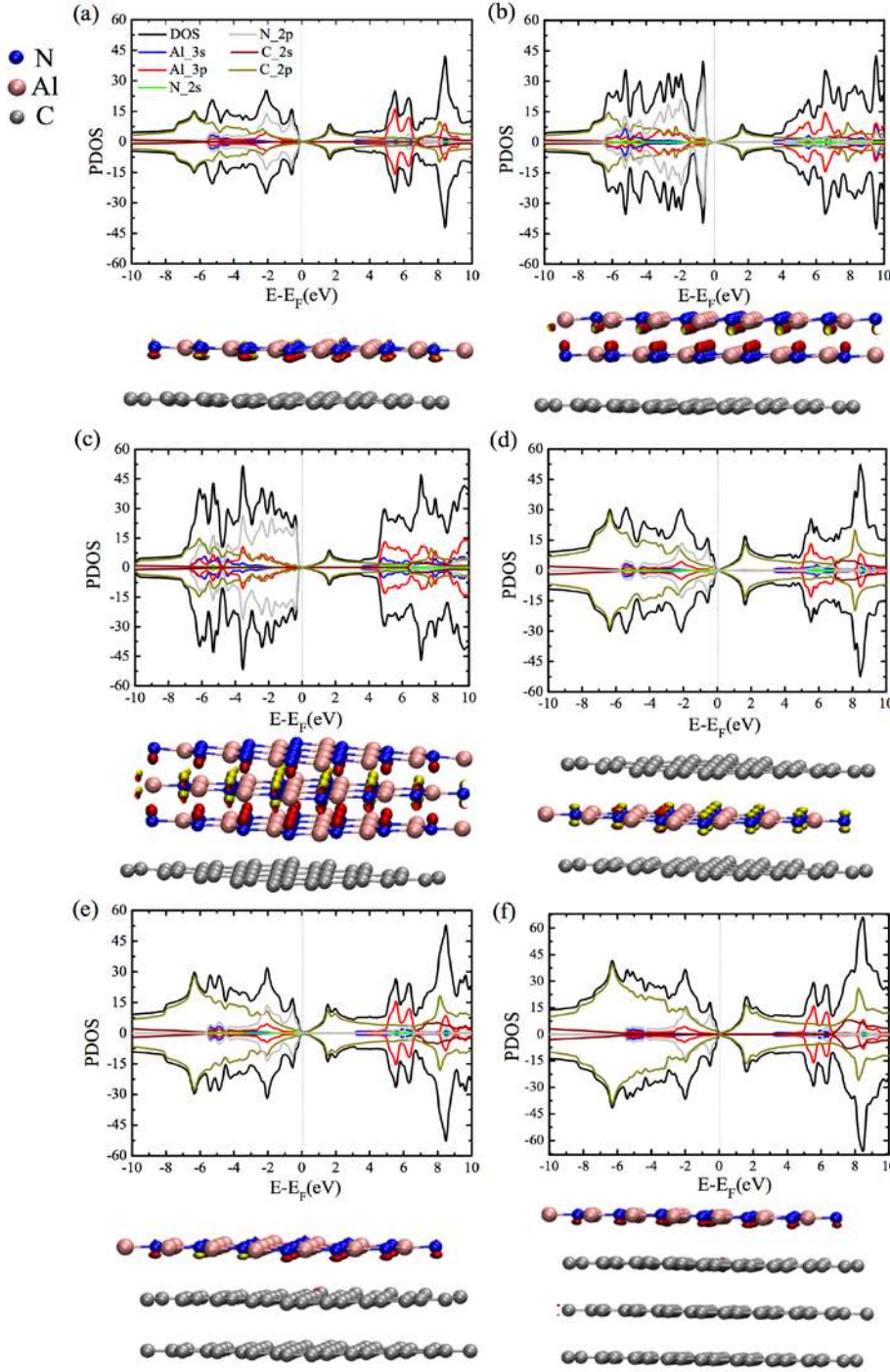
Figure 6. (a)–(f): Spin-polarized PDOS and the corresppponding electron density differences displayed below each of the PDOS graphs for stacks I–VI, following their representation in figure 3. In the electron density differences, the spin-up density is depicted in yellow while the spin-down density in shown in red.

Upon adding a second h-AlN layer on top of the first h-AlN layer thus assembling stack II, due to the h-AlN – h-AlN inter-layer interaction (which is stronger than the interaction h-AlN–graphene), the localization of the electron density becomes concentrated between the two h-AlN layers (figure 6(b)). This accounts for the increment of the electric dipole moment in the z-direction from 3.60 D to 3.69 D (table 3). Yet, if an extra h-AlN layer is added, thus assembling stack III, the localization of the electron density difference now becomes concentrated prevalently between two couples of h-AlN layers. This further reduces the interaction of the h-AlN layers with the graphene substrate (figure 6(c)). A general conclusion inferred from the analysis of the electronic structure of all stacks (I-VI) is that graphene behaves as a suitable substrate for h-AlN stacks. In the specific case of stack III, the additional h-AlN layer accounts for stronger polarization of the entire stack, and correspondingly for larger dipole moment of 4.07 D.

In the specific case of the stack IV (figure 6(d)), the electron density localization is equally distributed on both sides of the single-layer h-AlN, which naturally leads to vanishing of the electric dipole moment of the stack.

Finally, following a similar trend, by increasing the number of graphene layers, thus assembling stacks V and VI, we find that the electron density localization is between the h-AlN and graphene layers that between adjacent graphene layers. In these cases, somewhat larger components of electric dipole moments equal to 4.17 D and 4.38 D were calculated (table 3).

4. Conclusions

Our theoretical results, based on density-functional calculations combined with van der Waals corrections indicate that the dynamically stable single-layer h-AlN forms energetically favorable few-layer stacks with graphene. Our results point out that the interaction between two adjacent layers of h-AlN in such stacks is stronger, and the inter-layer distance of 2.18 Å is significantly shorter than that between adjacent layers of h-AlN and graphene or two adjacent graphene layers. Importantly, as seen from the analysis of the calculated PDOS, the electron density of the h-AlN layers is not significantly modified by stacking them in few-layer stacking sequences with graphene.

The specific stack comprising single-layer h-AlN sandwiched between two graphene layers achieves reliable chemical isolation of the h-AlN layer, thus adding to its stability and chemical inertness. Remarkably, stacks of few-layer h-AlN with graphene exhibit a significant (3.60 D –

4.38 D, depending on the particular stacking configuration) electric dipole moment component in the perpendicular direction to the atomic plane, resulting in an interface dipole. This dipole moment increases with the number of graphene or h-AlN layers in the stack and may be behind the physical mechanism responsible for the structural relaxation of h-AlN to wz-AlN. In addition, the interface dipole certainly has implications on both the reactivity and the adhesion properties of the stacks.

Acknowledgements

References

[1] I. Akasaki and H. Amano, Jpn. J. Appl. Phys. 36 (1997) 5393

[2] D. Ehrentraut and Z. Sitar, MRS Bulletin 34 (2009) 259

[3] A. Kakanakova-Georgieva, D. Nilsson, and E. Janzén, J. Cryst. Growth 338 (2012) 52

[4] O. Ambacher, Journal of Physics D: Applied Physics 31 (1998) 2653

[5] P. Tsipas, S. Kassavetis, D. Tsoutsou, E. Xenogiannopoulou, E. Golias, S. A. Giamini, C. Grazianetti, D. Chiappe, A. Molle, M. Fanciulli, and A. Dimoulas, Appl. Phys. Lett. 103 (2013) 251605

[6] V. Mansurov, T. Malin, Yu. Galitsyn, K. Zhuravlev, J. Cryst. Growth 428 (2015) 93

[7] A. Pakdel, Y. Bando, and D. Golberg, Chem. Soc. Rev. 43 (2014) 934

[8] C.L. Freeman, F. Claeyssens, N.L. Allan, and J.H. Harding, Phys. Rev. Lett. 96 (2006) 066102

[9] C. Bacaksiz, H. Şahin, H. D. Ozaydin, S. Horzum, R. T. Senger, and F. M. Peeters, Phys. Rev. B 91 (2015) 085430

[10] E.F. Almeida, F. Brito Mota, C.M.C. Castilho, A. Kakanakova-Georgieva, and G.K. Gueorguiev, Eur. Phys. J. B 85 (2012) 48

[11] Y. Jiao, A. Du, Z. Zhu, V. Rudolph, and S.C. Smith, J. Phys. Chem. C 114 (2010) 7846

[12] S.-S. Li, C.-W. Zhang, R.-W. Zhang, P. Li, F. Li, M. Yuan, M.-J. Ren, W.-X. Ji and P.-J. Wang, RCS Adv. 4 (2014) 7500

[13] J. Kim, C. Bayram, H. Park, C.-W. Cheng, C. Dimitrakopoulos, J.A. Ott, K.B. Reuter, S.W. Bedell, and D.K. Sadana, Nature Commun. 5 (2014) 4836

[14] Z. Y. Al Balushi, T. Miyagi, Y-C. Lin, K. Wang, L. Calderin, G. Bhimanapati, J. M. Redwing, J. A. Robinson, Surface Science 634 (2015) 81

[15] E. Artacho, E. Anglada, O. Diéguez, J.D. Gale, A. García, J. Junquera, R.M. Martin, P. Ordejón, J.M. Pruneda, D. Sánchez-Portal, and J.M. Soler, Journal of Physics. Condensed Matter 20 (2008) 064208

[16] J.P. Perdew, K. Burke, and M. Ernzerhof, Phys. Rev. Lett. 77 (1996) 3865

[17] N. Troullier, J.L. Martins, Phys. Rev. B 43 (1991) 8861

[18] S. Grimme, Journal of Computational Chemistry 27 (2006) 1787

[19] Jamie H. Warner, Mark H. Rummeli, Alicja Bachmatiuk, and Bernd Buechner, ACS Nano 4 (2010) 299

[20] J.D. Pack, H.J. Monkhorst, Phys. Rev. B 16 (1977) 1748

[21] A. Hansson, F. de Brito Mota, R. Rivelino, Phys. Rev. B 86 (2012) 195416

[22] H. Şahin, S. Cahangirov, M. Topsakal, E. Bekaroglu, E. Akturk, R.T. Senger, and S. Ciraci, Phys. Rev. B 80 (2009) 155453

[23] F.M. Morales, J.M. Mánuel, R. García, B. Reuters, H. Kalisch, and A. Vescan, J. Phys. D: Appl. Phys. 46 (2013) 245502

[24] G. Graziano, J. Klimeš, F. Fernandez-Alonso, A. Michaelides, J.Phys.: Condens. Matter 24 (2012) 424216

[25] M. Topsakal, E. Aktürk, S. Ciraci, Physical Review B 79 (2009) 115442

[26] A.H. Castro Neto, N.M.R. Peres, K.S. Novoselov, and A.K. Geim, Reviews of Modern Physics 81 (2009) 109

[27] D. Xu, H. He, R. Pandey, S.P. Karna, Journal of Physics. Condensed Matter : An Institute of Physics Journal 25 (2013) 345302

[28] W. Norimatsu and M. Kusunoki, Phys. Chem. Chem. Phys. 16 (2014) 3501

[29] G. Gao, W. Gao, E. Cannuccia, J. Taha-Tijerina, L. Balicas, A. Mathkar, T. N. Narayanan, Z. Liu, B. K. Gupta, J. Peng, Y. Yin, A. Rubio, and P. M. Ajayan, Nano Lett. 12 (2012) 3518

[30] R. Balu, X. Zhong, R. Pandey, S.P. Karna, Applied Physics Letters 100 (2012) 052104

[31] H. Liu, J. Gao, J. Zhao J. Phys. Chem. C 117 (2013) 10353−10359

[32] J. Xue, J. Sanchez-Yamagishi, D. Bulmash, P. Jacquod, A. Deshpande, K. Watanabe, T. Taniguchi, P. Jarillo-Herrero, B. J. LeRoy, Nat. Mater. 10 (2011) 282